
UniBrain: Universal Brain MRI Diagnosis with Hierarchical Knowledge-enhanced Pre-training

Jiayu Lei^{1,2}, Lisong Dai⁴, Haoyun Jiang^{3,2}, Chaoyi Wu^{3,2}, Xiaoman Zhang^{3,2}, Yao Zhang²
Jiangchao Yao^{3,2,†}, Weidi Xie^{3,2}, Yanyong Zhang¹, Yuehua Li⁴, Ya Zhang^{3,2}, Yanfeng Wang^{3,2,†}

misslei@mail.ustc.edu.cn

¹University of Science and Technology of China

²Shanghai AI Laboratory

³Shanghai Jiao Tong University

⁴Shanghai Sixth People's Hospital Affiliated to Shanghai Jiao Tong University

<https://github.com/ljy19970415/UniBrain>

Abstract

Magnetic resonance imaging (MRI) have played a crucial role in brain disease diagnosis, with which a range of computer-aided artificial intelligence methods have been proposed. However, the early explorations usually focus on the limited types of brain diseases in one study and train the model on the data in a small scale, yielding the bottleneck of generalization. Towards a more effective and scalable paradigm, we propose a hierarchical knowledge-enhanced pre-training framework for the universal brain MRI diagnosis, termed as UniBrain. Specifically, UniBrain leverages a large-scale dataset of 24,770 imaging-report pairs from routine diagnostics. Different from previous pre-training techniques for the unitary vision or textual feature, or with the brute-force alignment between vision and language information, we leverage the unique characteristic of report information in different granularity to build a hierarchical alignment mechanism, which strengthens the efficiency in feature learning. Our UniBrain is validated on three real world datasets with severe class imbalance and the public BraTS2019 dataset. It not only consistently outperforms all state-of-the-art diagnostic methods by a large margin and provides a superior grounding performance but also shows comparable performance compared to expert radiologists on certain disease types.

1 Introduction

Due to the benefit of the non-invasive nature and superior soft tissue contrast [31, 22], magnetic resonance imaging (MRI) has been considered as a reliable imaging method for brain disease diagnosis. With the rich morphological views of MRI modalities, *e.g.*, T1-Weighted Imaging (T1WI), T2-Weighted Imaging (T2WI), T2-Weighted Fluid Attenuated Inversion Recovery (T2FLAIR), and Diffusion-Weighted Imaging (DWI), clinicians can effectively diagnose a wide range of brain diseases such as glioma, brain hemorrhage, and acute cerebral infarction [21]. To save human labor and source, the computer-aided way draws more attention with the development of artificial intelligence.

Recently, deep learning has achieved an impressive performance on brain MRI data. For example, the deep learning models in [4, 1] have shown non-inferior diagnostic capability to human experts on Alzheimer disease diagnosis or glioma segmentation. Nevertheless, these early works [20, 50, 34] usually focus on the specific brain diseases of a few types and the models are trained on datasets in a

†: Corresponding author.

small scale, maintaining a weak generalization on more brain diseases. As the pre-training paradigm becomes prevalent to address this dilemma, how to build a framework for effective and scalable multi-disease diagnosis remains open and draws an increasing attention, *e.g.*, the recent studies for chest X-ray [46, 40]. However, currently, the pre-training models for the multimodal brain MRI data have not yet well considered [31, 22].

Towards the pre-training on brain MRI data, there are actually several challenges: 1) *sufficient available data*. The annotation in the field of brain diagnosis is always expensive and time-consuming, which leads to a lack of large-scale datasets that encompass a wide range of brain diseases and MRI modalities; 2) *specific domain knowledge*. The complex nature of brain diseases necessitates a profound understanding of various MRI modalities and their corresponding disease manifestations in a fine-grained granularity, which promotes the efficiency of pre-training; 3) *interpretable prediction*. As the typical diagnosis coexists with visual evidences, it is better for a framework to have some visual grounding along with the prediction, which helps radiologists understand the system and build the trust between humans and machines [40].

In this paper, we collect a large-scale brain MRI dataset that contains 24,770 imaging-report pairs of diverse brain diseases, and propose a knowledge-enhanced pre-training framework for the brain MRI diagnosis. Specifically, our design intuition builds upon a specific observation: the brain MRI report is composed of fine-grained components corresponding to each MRI modality, and coarse-grained conclusion of their union. This essentially provides us the potential to construct a hierarchical mechanism to strengthen the pre-training efficiency. Besides, given the diverse disease types and the rich MRI modalities, it is possible to pursue a universal paradigm with the strong generalization by encoding the commonality of brain diseases from both vision and text information. In summary, our contribution can be categorized as follows:

- We propose a novel hierarchical knowledge-enhanced pre-training framework that learns on a large-scale brain MRI dataset to pursue universal brain disease diagnosis.
- We design an automatic report decomposition for the fine-grained vision-language alignment to improve pre-training, and build a coupled perception module that can diagnose any brain disease with the proper description.
- We conduct extensive experiments to verify the effectiveness of the proposed architecture, and compare with many state-of-the-art (SOTA) pre-training algorithms on public BraTS2019 dataset and three in-house datasets. Our model not only consistently achieves the superior performance to the baselines *w.r.t.* the brain disease diagnosis and grounding but also yields comparable diagnosis performance compared to expert radiologists on certain disease types.

The rest of this paper is organized as follows: Section 2 presents related works. Section 3 describes in detail the proposed UniBrain pre-training framework. In Section 4, extensive experiments on three real world datasets and BraTS2019 are conducted to demonstrate the effectiveness of our pre-training model with ablation study in Section 5 explains the impact of submodules. Section 6 discusses advantages and limitations of the proposed method. We conclude our work in Section 7.

2 Related Work

2.1 Deep Learning in Brain MRI Diagnosis

In recent years, many deep learning methods have been proposed for the medical applications on brain MRI. According to the brain diseases of interests, existing works can be mainly summarized into three types: 1) *for brain tumors*. The brain tumor segmentation tasks with MRI have been well studied. Many works follow the framework of UNETR [14] and explore the improvement of the encoder structure [41, 26, 42, 47, 23, 7]. 2) *for stroke*. Automated segmentation and classification of images in the time-critical pathology is critical and practical. In this spirit, deep learning for abnormality detection and segmentation in lacunar and acute cerebral infarction has drawn much attention [25, 45]. 3) *for Alzheimer’s disease*. Recently, there are several arts devoted to Alzheimer’s disease diagnosis [20, 4], which have achieved impressive performance. For example, the deep learning models in [4] have shown non-inferior diagnostic capability to human experts on Alzheimer’s disease diagnosis. Despite effectiveness, these studies pay attention to a limited range of brain diseases.

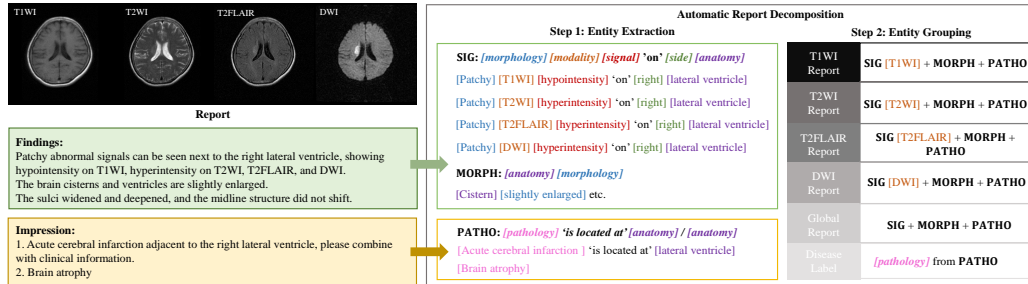


Figure 1: The brain MRI report example and its decomposition. Specifically, we design an automatic report decomposition pipeline to extract modality-wise and global MRI report (including the disease labels) from the vanilla MRI report findings and report impression.

In contrast, our UniBrain targets to offer universal diagnosis of diverse brain diseases via a pre-training framework.

2.2 Knowledge-enhanced Pre-training in Medical Domain

As vision-language pre-training (VLP) has achieved significant performance in the general domain, a range of explorations in the perspective of pre-training have been conducted to improve the performance of medical applications [39, 43]. Generally, these works can be summarized into two categories: the model architecture design and the data augmentation. For the former style, the domain knowledge including the principles of radiology and diagnostics are used to guide the design of the model structure, which makes the learning more efficient on the medical data [17, 24, 38, 12, 28]. For the latter style, the auxiliary medical data or description knowledge will be involved into the training [33, 44, 18, 8, 48, 6, 16, 40, 46]. For instance, MedKLIP [40] leverages the knowledge disease description to enhance the pre-training and outperform the previous SOTA on zero-shot diagnosis and grounding on chest X-ray. KAD [46] integrated a well-established medical knowledge graph to enhance the self-supervised training, which greatly improves the generalization ability and acquire the SOTA zero-shot results on all public chest X-ray data. Nevertheless, when it comes to the brain diseases, there is a lack of sufficient study of pre-training to show the promise. Especially, the brain MRI data contains multiple modalities, which is different from the chest-xray and requires the specific consideration in design.

3 Method

In this section, we will first introduce the preliminary and discuss our motivation in utilizing the report information for pre-training. Then, we will present our automatic report decomposition strategy and hierarchical knowledge-enhanced pre-training framework sequentially.

3.1 Problem Statement

Let $D_{\text{train}} = \{(x^1, r^1), \dots, (x^N, r^N)\}$ denote a collection of N image-report pairs, where each x is a collection of K MRI modalities, *i.e.*, $x = (x_1, \dots, x_K)$, and r refers to the corresponding MRI case report. Our goal is to construct a pre-training framework for universal brain disease diagnosis.

After pre-training, we can infer the likelihood of the brain diseases given a disease query set Q , namely, $p = f(x, Q)$.

3.2 Motivation

Pioneering works have proved the effectiveness of incorporating the radiology report into visual-language pre-training (VLP) in medical field [46, 40, 16, 2, 48]. Nevertheless, previous methods are mainly developed for chest X-ray [46, 40, 32, 19, 27, 29], whose report corresponds to single chest X-ray imaging. In comparison, brain MRI report contains information for multi-modal imagings, so the VLP methods on unimodal chest X-ray is not efficient for brain MRI.

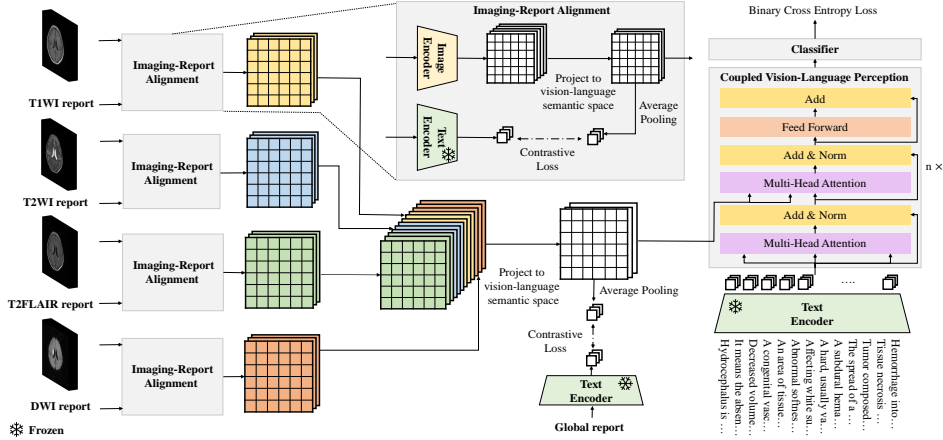


Figure 2: The illustration of our pre-training framework UniBrain. We utilize four transverse MRI modalities, namely T1WI, T2WI, T2FLAIR, DWI, and case reports to train UniBrain. In this framework, we first align the modality-wise imaging-report feature, then we project the concatenated features to vision-language semantic space, and align the global imaging-report feature. Finally, the global image feature acts as the key and value, and the disease description set acts as the query for the coupled vision-language perception module to produce the final multi-class classification.

We present an example of the brain MRI report in Fig. 1 (left), which consists of two components: *report findings* and *report impression*. As shown in report findings, we can find the information focus on different aspects. For example, signal intensities directly correlate to each modality from the description “patchy abnormal signals can be seen next to the right lateral ventricle, showing hypointensity on T1WI, hyperintensity on T2WI, T2FLAIR, and DWI” or morphology changes on different anatomies from “the brain cisterns and ventricles are slightly enlarged” and “the sulci widened and deepened”. In report impression, it provides the disease conclusion and the corresponding located anatomies *e.g.*, “Acute cerebral infarction adjacent to the right lateral ventricle”.

Motivated by this observation in the MRI report, we propose to decompose the report into some structured formats and build a hierarchical knowledge-enhancement for pre-training.

3.3 Automatic Report Decomposition

As shown in Fig. 1, we propose an automatic report decomposition (ARD) pipeline, which consists of two steps: 1) *entity extraction*. Extract the most critical entities according to radiologist experience and reformulate them into structured formats; 2) *entity grouping*. Assign the structured sentences into modality-wise and global reports, and further get the disease labels for classification. Then, the reports will be applied in the proposed pre-training architecture in Fig. 2.

3.3.1 Entity Extraction

In this step, we aim to select informative entities from the report to avoid the interference of extraneous words and complex grammar. Specifically, we follow the radiologist experience to define 6 kinds of entities, *i.e.*, *anatomy*, *side*, *modality*, *signal*, *morphology*, and *pathology*.

Then, given a brain MRI report r with a set of sentences, *i.e.* $r = \{s_1, s_2, \dots, s_M\}$, we independently extract entities for each sentence, and convert the sentence to one of the following structured formats: 1) SIG = $\{[morphology] [modality] [signal] 'on' [side] [anatomy]\}$, which indicates the information about modality signal, such as ‘Patchy DWI hyperintensity on right lateral ventricle’; 2) MORPH = $\{[anatomy] [morphology]\}$, which captures morphological changes on anatomies such as ‘The sulci widened’; 3) PATHO = $\{[pathology] 'is located at' [anatomy]\}$, which reflects pathological changes such as ‘Acute cerebral infarction is located at lateral ventricle’. Note that, when any certain entity type in SIG, MORPH or PATHO is absent, we will replace it with an empty string.

If no anatomy is specified, PATHO follows $\{[pathology]\}$.

3.3.2 Entity Grouping

This step correlates each structured sentence with modalities so that we can build a hierarchical (modality-wise and global) enhancement to improve pre-training. Specifically, let $\bar{r} = \{\bar{s}_1, \bar{s}_2, \dots, \bar{s}_M\}$ denote the structured report after the *entity extraction* step. For each \bar{s}_m , if it follows the SIG format, we then add it to the corresponding modality-wise collection \bar{r}_k following the rule as below:

$$\bar{r}_k \leftarrow \bar{r}_k \cup \{\bar{s}_m\}, \text{ if modality } k \text{ occurs in } \bar{s}_m. \quad (1)$$

If it follows MORPH or PATHO format, we add it to every modality-wise collection following another rule as below:

$$\bar{r}_k \leftarrow \bar{r}_k \cup \{\bar{s}_m\}, \forall k \in \{1, 2, \dots, K\}. \quad (2)$$

After ARD, we can acquire the structured modality-wise reports $\{\bar{r}_1, \bar{r}_2, \dots, \bar{r}_K\}$ and global report \bar{r} , which are used in the following pre-training.

3.4 Hierarchical Knowledge-enhanced Pre-training

Considering the characteristic of brain MRI data, we propose a hierarchical knowledge-enhanced pre-training framework, which consists of three important components: 1) the *modality-wise imaging-report alignment* promotes the modality-wise knowledge efficiently encoded into the modality representation; 2) the subsequent *global imaging-report alignment* strengthens the interaction of multiple modality representations, yielding a more comprehensive merged representation; 3) the final *coupled vision-language perception* module compatible with the universal brain disease, and progressively matches the imaging patches with a disease query to generate the fine-grained grounding and the coarse-grained diagnosis.

The details are as follows. First, regarding the imaging modalities, as the abnormal signal intensities have same definition, we use a shared image encoder to extract the modality-wise visual representation. Concretely, we denote the latent visual representation of each modality as follows,

$$\mathbf{u}_k = \phi_{\text{proj}}(\phi_{\text{image}}(x_k)) \in \mathbb{R}^{l \times d}, k \in \{1, 2, \dots, K\}, \quad (3)$$

where $\phi_{\text{image}}(\cdot)$ follows the structure of ResNet3D [36] and we adopt the output of the penultimate layer as the original image patch embedding, $\phi_{\text{proj}}(\cdot)$ is a Multilayer Perceptron (MLP) to project the original image patch embedding to the vision-language semantic space, l denotes the image patch number and d is the embedding dimension of each image patch.

Regarding the report information, we use a text encoder to extract the modality-wise and global report features as below,

$$\begin{aligned} \mathbf{v}_k &= \phi_{\text{text}}(\bar{r}_k) \in \mathbb{R}^d, k \in \{1, 2, \dots, K\}, \\ \mathbf{v} &= \phi_{\text{text}}(\bar{r}) \in \mathbb{R}^d. \end{aligned} \quad (4)$$

To leverage the relationship among medical entities, we use a MedKEBERT [13] pretrained on Unified Medical Language System (UMLS) data [46] as $\phi_{\text{text}}(\cdot)$, and freeze its parameters.

3.4.1 Modality-wise Imaging-report Alignment

In this component, we perform a modality-wise alignment between \mathbf{u}_k and \mathbf{v}_k ($k \in \{1, 2, \dots, K\}$) as shown in Fig. 2. Intuitively, by leveraging modality-wise report reference, the modality-wise vision clues can be sufficiently distilled into the corresponding representation. Given a minibatch of B imaging-report pairs, the modality-wise alignment is conducted in the following

$$\ell_k = \frac{1}{B} \sum_{i=1}^B \frac{1}{\Omega(i)} \left(\ln \frac{e^{\hat{\mathbf{u}}_k^{i\top} \mathbf{v}_k^i / \tau}}{\sum_{j=1}^B e^{\hat{\mathbf{u}}_k^{i\top} \mathbf{v}_k^j / \tau}} + \ln \frac{e^{\mathbf{v}_k^{i\top} \hat{\mathbf{u}}_k^i / \tau}}{\sum_{j=1}^B e^{\mathbf{v}_k^{i\top} \hat{\mathbf{u}}_k^j / \tau}} \right), \quad (5)$$

In MRI imaging, hyperintensity always means abnormally higher signal intensities and hypointensity always means abnormally lower signal intensities, which applies to all MRI modalities.

where $\Omega(i)$ measures the number of reports same to the i -th report in the mini-batch, $\hat{\mathbf{u}}_k^i = \phi_{\text{pool}}(\mathbf{u}_k^i) \in \mathbb{R}^d$ that pools the embedding along the patch dimension for each k -th modality imaging, and τ is the learnable temperature parameter. Note that, we follow the CLIP loss [30] to build a formulation of bidirectional contrast learning, namely, one image-to-text contrast term and one text-to-image contrast term in Eq. (5).

3.4.2 Global Imaging-report Alignment

In this global imaging-report alignment, we first summarize the modality-wise feature evidences, *i.e.*, $\{\mathbf{u}_1, \mathbf{u}_2, \dots, \mathbf{u}_K\}$, to acquire a global feature vector \mathbf{u} , which is modeled by the the following projection

$$\mathbf{u} = \phi_{\text{fuse}}(\mathbf{u}_1, \mathbf{u}_2, \dots, \mathbf{u}_K) \in \mathbb{R}^{l \times d}. \quad (6)$$

where $\phi_{\text{fuse}}(\cdot)$ is a linear neural layer mapping one input in $\mathbb{R}^{l \times K \times d}$ to one output in $\mathbb{R}^{l \times d}$. Then, together with the previous global report embedding \mathbf{v} , we can perform a contrastive learning similar to Eq. (5) but in a global view. The loss for the global imaging-report alignment can be formulated as follows

$$\ell_g = \frac{1}{B} \sum_{i=1}^B \frac{1}{\Omega(i)} \left(\ln \frac{e^{\hat{\mathbf{u}}^i \top \mathbf{v}^i / \tau}}{\sum_{j=1}^B e^{\hat{\mathbf{u}}^i \top \mathbf{v}^j / \tau}} + \ln \frac{e^{\mathbf{v}^i \top \hat{\mathbf{u}}^i / \tau}}{\sum_{j=1}^B e^{\mathbf{v}^i \top \hat{\mathbf{u}}^j / \tau}} \right), \quad (7)$$

where $\Omega(i)$ is same to that in Eq. (5) and $\hat{\mathbf{u}}^i = \phi_{\text{pool}}(\mathbf{u}^i) \in \mathbb{R}^d$ that pools the global embedding along the patch dimension. By performing such a global alignment, we can efficiently learn complex disease patterns beyond the modal-wise evidences.

3.4.3 Coupled Vision-Language Perception

Regarding the diagnosis component, instead of the straightforward discriminative prediction, we adopt a coupled vision-language perception module (CVP) via a transformer decoder-based structure [37] as shown in Fig. 2. Specifically, we use the global imaging embedding \mathbf{u} as key, value and use the pre-trained text encoder mentioned in previous sections to encode the disease descriptions \mathbf{Q} as queries. The disease-attentive embedding for the brain MRI on the disease set \mathbf{Q} is generated as follows

$$\mathbf{h} = \phi_{\text{CVP}}(\mathbf{u}, \phi_{\text{text}}(\mathbf{Q})) \in \mathbb{R}^{C \times d}, \quad (8)$$

where $Q = \{q_1, \dots, q_C\}$ is a collection of disease descriptions generated by UMLS, C is the number of queried diseases, and $\phi_{\text{CVP}}(\cdot, \cdot)$ is the transformer decoder. Note that, such a design enjoys two merits: 1) we can apply any type of brain disease if it can be expressed by UMLS with the proper descriptions. This aligns our goal about the universal brain diagnosis. 2) In the progressive transformation with the attention mechanism, the response of each image patch can be explicitly characterized, which provides us some evidence about some specific disease. Specially, we can visualize the class activation map (CAM) [49] on the latent patch features to make the diagnosis attribution. Finally, \mathbf{h} is fed to a classifier to output a prediction $p \in \mathbb{R}^C$ for C diseases. The classification loss is formulated in the following

$$\ell_{\text{bce}} = \frac{1}{B} \sum_{i=1}^B \frac{1}{C} \sum_{c=1}^C (y_c^i \ln p_c^i + (1 - y_c^i) \ln(1 - p_c^i)), \quad (9)$$

where $[p_1, p_2, \dots, p_C] = \phi_{\text{classifier}}(\mathbf{h})$ modeled by an MLP layer, and y^i reflects whether the report impression has the corresponding pathology.

3.4.4 Training, Inference and Beyond

In the aforementioned subsections, we proposed three losses corresponding to different roles in hierarchical knowledge enhanced pre-training. Putting all together, our training objective is formulated as

$$\mathcal{L} = \ell_{\text{bce}} + \frac{1}{K+1} \left(\ell_g + \sum_{k=1}^K \ell_k \right). \quad (10)$$

After ARD, there are some structured reports that can be totally same. This term guarantees to debias cross positive pairs in the mini-batch if repeated structured reports exists, otherwise $\Omega(i) = 1$.

Note that, in the above equation, we have not introduced hyperparameters to balance different loss terms. This is because that we find maintaining them equally can work well. We tried to balance loss terms with different weights, which is comparable or not better than Eq. (10). During inference phase, we can directly manipulate the diseases of interest with the proper description in Q , and forward to UniBrain to have the predictions. Besides, as our ϕ_{CVP} is based on transformer decoder structure, one can input queries of any length without changing the pre-trained weights of UniBrain, making it easy for zero-shot diagnosis on unseen categories. When fine-tuning on the downstream dataset, one can accordingly modify the disease query set and train the networks with or without ℓ_g and ℓ_k depending on whether the report is available. The results in the following section will sufficiently demonstrate UniBrain can generalize well under open-class and domain shift.

4 Experiments

To evaluate our method, we conduct experiments on four diverse datasets of which three are real world medical imaging datasets, one is public dataset BraTS2019. We compare the method against multiple baselines to verify the diagnosis and generalization performance of UniBrain.

4.1 Datasets and Evaluation Metrics

4.1.1 Pre-training Dataset

- **Shanghai Sixth People’s Hospital Dataset (SSPH):** We collected 24,770 brain MRI imaging-report pairs at Shanghai Sixth People’s Hospital in the study. Here, all MRI scans were performed on one of the eight MRI scanners (GE Medical Systems Signa Pioneer, Philips Medical Systems EWS, Philips Medical Systems Ingenia, Siemens Prisma, Siemens Skyra, Siemens Verio, UIH uMR 780, UIH uMR 790) from January 2019 to March 2023 at Shanghai Sixth People’s Hospital. Each data has a case report and four transverse MRI modalities: T1WI, T2WI, T2FLAIR and DWI. The dataset has 13 categories: normal, lacunar cerebral infarction, brain atrophy, white matter lesions, acute cerebral infarction, chronic cerebral infarction, metastasis, brain hemorrhage, epidura and subdural hemorrhage, meningioma, hemangioma, glioma and hydrocephalus. The category distribution is severely imbalanced as shown in Fig. 3. Note that, such an imbalanced distribution is common in real-world hospital data due to the disease morbidity and the specialization of hospitals in diagnosing diseases.

4.1.2 Downstream Datasets

- **BraTS2019 Dataset:** We use the BraTS2019 dataset [10] that has four MRI modalities: T1WI, T2WI, T2FLAIR, and T1 contrast-enhanced (T1CE), to test the zero-shot or finetuning performance of UniBrain. There are 259 volumes of high-grade glioma (HGG) and 73 volumes of low-grade glioma (LGG), which can be directly used for zero-shot evaluation. Regarding the finetuning setting, we split BraTS2019 into training and testing under the ratio of 7:3 following the way in [5].
- **Affiliated Hospital of Nantong University Dataset (AHNU):** This dataset is collected from Affiliated Hospital of Nantong University, consisting of 706 MRI imagings under 4 modalities: T1WI, T2WI, T2FLAIR, DWI. It contains 13 categories same to those in our pre-training dataset. We mainly use this dataset to test the generalization ability of UniBrain under domain shift.
- **Wuhan Hankou Hospital Dataset (WHH):** It is collected from Wuhan Hankou Hospital, which has 618 MRI imagings of 13 categories in SSPH under 4 modalities: T1WI, T2WI, T2FLAIR, DWI. We use this dataset to test the generalization ability of UniBrain under domain shift.

This study has been approved by the Ethics Committee of Shanghai sixth people’s Hospital [IRB code: 2023-KY-082 (K)].

This modality has not occurred on the SSPH dataset.

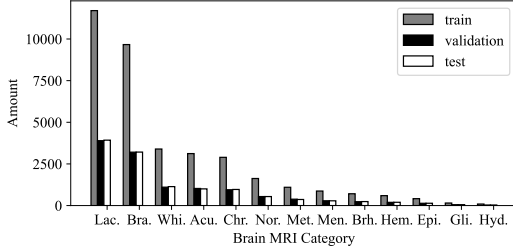


Figure 3: The category distribution of the train subset, the validation subset and the test subset in SSPH. The first three letters are used as the shorthand of each class except for “Brain Atrophy” and “Brain hemorrhage” that we denote by “Bra” and “Brh” respectively.

Method	2D/3D	Data Type	Multi-Modality	VLP
ConVIRT [48]	2D	X ray		✓
CheXZero [35]	2D	X ray		✓
MedKLIP [40]	2D	X ray		✓
KAD [46]	2D	X ray		✓
TransMed [11]	3D	MRI	✓	
DSM [5]	3D	MRI		
UniBrain	3D	MRI	✓	✓

Table 1: Setting Summary of UniBrain and baselines. The setting includes 2D/3D inputs, Data Type, Multi-modality, VLP. UniBrain is the first and “work using visual-language pre-training on 3D multi-modality brain MRI data.”

4.1.3 Evaluation Metrics

We respectively use area under curve (AUC), Accuracy (ACC), Average Precision (AP) and F1-score (F1) for each category and their average number, *i.e.* average AUC (aAUC), average Accuracy (aACC), average F1-score (aF1) and mean Average Precision (mAP), as our evaluation metrics. These metrics are calculated as follows:

$$\begin{aligned}
 \text{aAUC} &= \frac{1}{C} \sum_{c=1}^C \text{AUC}_c, \\
 \text{aACC} &= \frac{1}{C} \sum_{c=1}^C \frac{\text{TP}_c + \text{TN}_c}{\text{TP}_c + \text{FP}_c + \text{TN}_c + \text{FN}_c}, \\
 \text{aF1} &= \frac{1}{C} \sum_{c=1}^C \frac{2\text{TP}_c}{2\text{TP}_c + \text{FP}_c + \text{FN}_c}, \\
 \text{mAP} &= \frac{1}{C} \sum_{c=1}^C \text{AP}_c,
 \end{aligned} \tag{11}$$

where TP_c , FN_c , TN_c , FP_c denote number of true positive, false negative, true negative, false positive samples for the c -th category respectively, and AUC_c , AP_c are the common AUC performance and AP performance of the c -th category that can be easily calculated in the standard python API.

4.2 Pre-training Details

SSPH is split into 3:1:1 for training, validation, and test, and each modality input is resized to $224 \times 224 \times 24$. For all our experiment, 3Dseg-8 pre-trained ResNet3D-34 [9] is used as the default image encoder of UniBrain. We will also discuss the impact of the image encoder in Section 5. The learnable temperature parameter τ is initialized the same as [46]. We set the number of Transformer decoder blocks in ϕ_{CVP} as 4 with 4 heads. For baselines in the experiments, we strictly followed the architectures described in the original papers.

Our UniBrain is implemented in Pytorch and trained with 2 NVIDIA A100 GPUs (each has 80GB memory) for 100 epochs from scratch with a batch size of 16. We adopt the Adam optimizer and its initial learning rate is set to 0.0002 with a poly learning rate schedule, in which the initial rate decays by each epoch with a power 0.9. For data augmentation, we use the following operations: (1) random mirror flipping across the axial, coronal and sagittal planes by a probability of 0.5; (2) random intensity shift in $[-0.1, 0.1]$ and scale in $[0.9, 1.1]$. The L2 Normalization is also applied for model regularization with a weight decay rate of $1e-5$.

Table 2: Comparison of UniBrain with the baselines in terms of aAUC, aACC, aF1 and mAP. We use the first three letters to represent each class except for “Brain Atrophy” and “Brain hemorrhage” that we use “Bra” and “Brh” respectively. Numbers within parentheses indicate 95% confidence intervals (CI) and the best results for each column are marked in bold.

Method	Lac.	Bra.	Whi.	Acu.	Chr.	Nor.	Met.	Brh.	Epi.	Men.	Hem.	Gli.	Hyd.	aAUC	aACC	aF1	mAP
ConvVIRT [48]	46.23	72.75	74.10	65.20	32.79	93.53	62.39	70.23	48.13	61.28	63.90	83.93	51.08	63.50	79.54	38.57	28.87
CheXZero [35]	34.45	86.71	78.53	41.59	30.83	87.95	67.94	62.66	55.06	60.85	57.67	79.81	85.66	63.83	76.63	36.16	27.51
TransMed [11]	83.81	91.25	85.91	70.97	77.41	91.10	56.63	57.19	62.09	59.48	54.83	69.00	67.77	71.34	81.48	36.08	32.77
MedKLIP [40]	88.06	91.22	91.33	90.56	81.86	95.24	77.82	82.89	78.33	75.61	68.66	81.26	88.18	83.93	89.17	48.87	45.88
KAD [46]	87.88	92.46	92.67	90.25	81.85	95.68	80.76	85.37	80.60	74.27	74.27	68.94	89.56	85.57	90.61	52.09	50.33
UniBrain	90.35	94.48	94.27	96.1	88.17	96.61	89.32	91.43	93.50	79.13	73.1	93.75	97.63	90.71	92.62	62.27	63.27
(95% CI)	(89.39, 93.85, 93.63, 95.42, 86.93, 96.09, 87.57, 89.27, 91.09, 76.46, 69.53, 89.74, 96.12, 91.30, 95.10, 94.91, 96.78, 89.40, 97.13, 91.07, 93.58, 95.90, 81.80, 76.67, 97.76, 99.13)	(91.31)	(93.16)	(63.82)	(65.11)												

4.3 Baselines

We consider a range of baselines in comparison: 1) multi-modal MRI classification model: TransMed [11]; 2) VLP models: ConVIRT [48], CheXZero [35], MedKLIP [40], KAD [46], which are the most advanced methods that apply VLP to medical domain. For the comparison on BraTS2019, we also include DSM [5] which achieves the best result on tumor classification on BraTS2019. Each method is introduced in the following and summarized in Table ??.

- **ConVIRT** [48] learns the medical visual representations through bidirectional contrast from the image-text pairs.
- **CheXZero** [35] fine-tunes the pre-trained CLIP model with the image-text pairs in the medical domain.
- **MedKLIP** [40] incorporates the specific medical domain knowledge to enhance the pre-training process.
- **KAD** [46] utilizes the medical knowledge graph to promote the VLP on chest X-ray data.
- **TransMed** [11] combines CNN and Transformer to improve the parotid gland tumor classification through multi-modal MRI imagings.
- **DSM** [5] uses two spatiotemporal models to classify different types of brain tumours, and has shown a promising and competitive performance on the BraTS2019 dataset.

4.4 Quantitative Results

Here, we first use the SSPH training set as the pre-training data for UniBrain and other baseline methods [48, 35, 11, 40, 46], and test their aAUC, aACC, aF1, and mAP on the SSPH test set. The results presented in Table 2 demonstrate the superior performance of UniBrain across all metrics examined.

4.4.1 UniBrain outperforms the SOTA diagnosis model

When compared to TransMed, another multi-modal MRI diagnosis model, UniBrain achieves significant improvements in aAUC, aACC, aF1, and mAP by 19.37%, 11.14%, 26.19%, and 30.5%, respectively. When compared to the SOTA VLP model KAD, our method outperforms it by 5.14%, 2.01%, 10.18%, and 12.94% in aAUC, aACC, aF1, and mAP, respectively. These results highlight the advantages of using multi-modal data in a hierarchical enhancement manner for pre-training.

4.4.2 UniBrain is robust to the imbalanced dataset

What is particularly noteworthy regarding UniBrain is its substantial improvement on aF1 and mAP when compared to the SOTA models. This shows the robustness of UniBrain when the dataset is quite imbalance like Fig. 3. In particular, UniBrain achieves significant improvements in eight minority disease types including acute cerebral infarction, chronic cerebral infarction, metastasis, brain hemorrhage, epidural and subdural hemorrhage, meningioma, glioma, and hydrocephalus, which comprise less than 20% of the entire dataset.

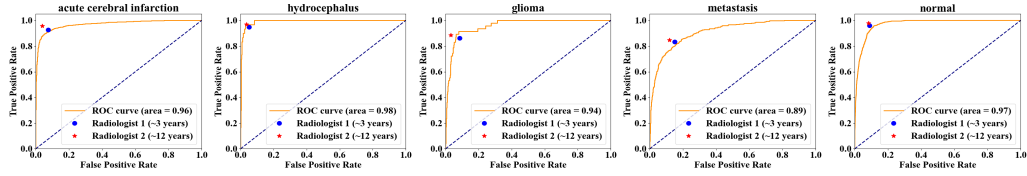


Figure 4: UniBrain achieves the comparable performance on five categories, namely, acute cerebral infarction, glioma, hydrocephalus, metastasis and normal, compared to two brain MRI radiologists with 3 and 12 years of clinical experience respectively.

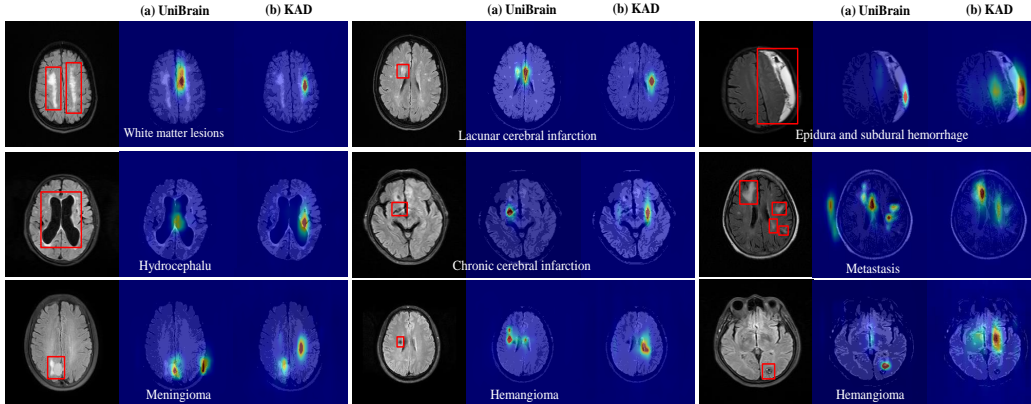


Figure 5: We present the original image (left) and the corresponding attention map generated by UniBrain (column (a)) and KAD (column (b)) respectively. In the original images, lesion areas annotated by radiologists are highlighted by red boxes. In the attention maps, a color spectrum ranging from red to blue is overlaid on the original image, where red represents regions of high attention and blue represents regions of low attention.

4.4.3 UniBrain is comparable to radiologists on certain categories

We invite two brain MRI radiologists with 3-year and 12-year clinical experience respectively as our human baseline on 13 categories. We find that UniBrain achieves the comparable results on 5 categories, namely, acute cerebral infarction, glioma, hydrocephalus, metastasis and normal compared to the radiologists as shown in Fig. 4. This result demonstrates the great potential for UniBrain to apply to the clinical diagnosis.

4.5 Qualitative Results

In Fig. 5, we visualize the classification clues by illustrating the original image and the corresponding attention map generated by UniBrain (shown in column (a)) and KAD (shown in column (b)) respectively. As can be seen, in the original images, lesion areas annotated by radiologists are highlighted by red boxes. In the attention maps, a color spectrum ranging from red to blue is overlaid on the original image, where red represents regions of high attention and blue represents regions of low attention. Notably, we observed that when different disease queries were inputted, compared to KAD, UniBrain generated attention maps that focused on disease-specific lesions more accurately. This grounding performance suggests that our hierarchical knowledge-enhanced framework does improve the pre-training performance with the merits of interpretation, which is essential for AI-assisted applications. With this, clinicians can better understand AI predictions and make collaboration in the computer-aided clinical diagnosis.

Table 3: Comparison of UniBrain with SOTA medical pre-training models on two external in-house datasets. ZS means zero-shot result. The best results are in bold.

Method	AHNU				WHH			
	aAUC	aACC	aF1	mAP	aAUC	aACC	aF1	mAP
MedKLIP-ZS [40]	62.00	54.67	39.89	33.47	59.04	48.62	37.99	30.68
TransMed-ZS [11]	67.96	62.72	41.77	36.98	65.37	61.72	41.29	34.78
KAD-ZS [46]	77.29	73.25	50.52	46.38	78.44	75.34	52.48	47.58
UniBrain-ZS	86.23	87.03	61.82	62.13	86.50	85.87	62.87	60.09

Table 4: Comparison between Finetuned UniBrain (termed as UniBrain-FT) and previous SOTA method DSM [5] on BraTS2019 and the zero-shot comparison between UniBrain (marked as UniBrain-ZS) and KAD (marked as KAD-ZS). For DSM, we use the paper’s result. The best results are in bold.

Method	BraTS2019			
	aAUC	aACC	aF1	mAP
DSM [5]	-	-	90.36	-
KAD-ZS [46]	50.52	51.48	62.54	50.27
UniBrain-ZS	62.77	59.11	64.88	58.09
UniBrain-FT	94.29	93.75	91.97	94.03

4.6 Generalization

4.6.1 Generalization on the open-class setting

We further verify UniBrain under the open-class setting with BraTS2019. Specifically, we compared the performance of UniBrain on diagnosing HGG and LGG with that of the SOTA method DSM [5] in Table 4. We use the same training and test set reported in DSM paper and thus derive the DSM baseline from the reported results (only F1 score is reported) in the original paper. It is important to note that LGG and HGG on BraTS2019 have not appeared in the categories of our pre-training data, and T1CE modality of BraTS2019 is not used during our pre-training.

In addition, as there are no reports on BraTS2019, we only finetune UniBrain with ℓ_{bce} .

According to Table 4, UniBrain achieved a superior performance compared to KAD [46] under the zero-shot setting. Besides, UniBrain finetuned on BraTS2019 also surpassed DSM [5], showcasing its ability as a foundation model for open-class diagnosis.

4.6.2 Generalization on the domain shift setting

To study the performance of UniBrain under the domain shift setting, we verified the pre-training models on AHNU and WHH which have same categories as SSPH but with the covariate shift. We test the zero-shot results to assess the generalization ability of UniBrain compared with two VLP models and TransMed. Table 3 suggests the remarkable potential of UniBrain across different hospitals, which can be a promising prospect.

5 Ablation Study

In this section, we conduct a thorough ablation study for UniBrain to understand the performance impact of the individual components, namely, ARD, visual-language encoders and hierarchical knowledge-enhancement. The ablation results of different components are summarized in Table 6, which we will explain in details for each component in the following.

Please refer to the dataset description in the previous paragraph for details.

5.1 Effectiveness of Automatic Report Decomposition

5.1.1 Effectiveness of hierarchical report extraction

To show the effectiveness of the proposed ARD, we compare it with ChatGPT [3]. Specially, we provide the predefined decomposition examples as demonstrations to ask ChatGPT to perform the report decomposition, and provide the results in the rows *w.r.t.* “w/ chatGPT report” of Table 6. As can be seen, compared to ChatGPT [3], ARD shows the superior performance with increases in aAUC, aACC, aF1, and mAP by 0.93%, 0.15%, 0.75%, and 1.36% respectively. It suggests that the proper human experience and labor in the extraction make the report decomposition more informative and efficient.

5.1.2 Effectiveness of disease label extraction

As aforementioned in previous section, we directly generate the label for each MRI sample by checking whether the report impression contains the corresponding pathology. We verify our generation process with an evaluation set of 250 samples. In this set, experienced radiologists provided the gold standard disease labels for each imaging-report pair. The performance of ARD in disease label extraction was evaluated by comparing with the gold standard labels on the evaluation set, under on the tasks of mention and negation detection measured by the F1 score. Specially, mention detection should give a positive label if the gold standard shows the patient gets the certain disease, while negation detection should give a positive label if the gold standard shows the patient does not have the certain disease. The results in Table 5 reveal that ARD reaches a competitive precision in extracting disease labels from report impression.

5.2 Performance under Different Encoders

In UniBrain, we adopted ResNet3D 34 as the image encoder. Here, we verify the performance of ResNet3D 50 to see how network depth affects the results. Regarding the text encoder, we substitute MedKEBERT [46] in UniBrain with clinicalBERT which is pre-trained on clinical notes [15], to validate its efficiency. As shown in the rows *w.r.t.* encoders of Table 6 (w/ ResNet3D 50, w/ clinicalBERT), we can find that the depth 50 of image encoder does not show the significant different with the depth 34 in UniBrain. However, changing text encoder to clinicalBERT [15] leads to the degraded performance, since UMLS is a more structured knowledge corpora than clinical notes. This suggests pre-training the text encoder with the well-organized knowledge base is critical to enhance the VLP.

5.3 On Hierarchical Knowledge-enhancement

5.3.1 Effectiveness of hierarchical imaging-report alignment

As shown in Table 6, we can observe a significant drop in performance when all imaging-report alignments are absent, *i.e.* eliminating ℓ_g and all ℓ_k in Eq. (10). It suggests that the process of knowledge-enhancement helps learn better cross-vision-language representations, resulting in the improvement. Furthermore, when only keeping the global imaging-report alignment (*i.e.*, w/o modality-wise alignment), the results are better than removing all imaging-report alignments but worse than the complete UniBrain. This indicates the effectiveness of the hierarchical imaging-report alignment during pre-training.

5.3.2 Effectiveness of the coupled vision-language perception

Finally, we verified the effect of the CVP module in UniBrain. According to Table 6, removing CVP degrades the performance (w/o CVP) significantly in aF1 and mAP, which shows the importance of CVP in transforming the global image features into disease-specific classification features. Besides, we explore the impact of the query form for CVP by conducting an additional experiment with using the disease name instead of the disease description as Q . From the results of Table 6 *w.r.t.*, w/o disease description query, we can find that the model using the disease description as the query significantly outperforms the model using the disease name. We attribute this to the fact that the

An complete prompt follows this format: Report decomposition introduction # Decomposition demonstrations # Reports to be decomposed.

Table 5: The label extraction performance of ARD on the test set for mention and negation detection. The Macro-average and Micro-average rows are computed over all 13 classes.

Category	Mention F1	Negation F1
Lacunar cerebral infarction	100.00	100.00
Brain atrophy	100.00	100.00
White matter lesions	100.00	100.00
Chronic cerebral infarction	100.00	100.00
Normal	100.00	100.00
Metastasis	100.00	100.00
Hydrocephalus	100.00	100.00
Brain hemorrhage	81.25	98.74
Acute cerebral infarction	72.72	98.77
Epidura and subdural hemorrhage	96.43	99.56
Meningioma	95.65	99.57
Hemangioma	97.77	99.78
Glioma	92.31	99.79
Micro-average	97.32	99.70
Macro-average	95.09	99.71

Table 6: Ablation study of UniBrain. The best results are in bold.

Methods	aAUC	aACC	aF1	mAP
Ablation of ARD				
w/ chatGPT report	89.78	92.47	61.52	61.91
Ablation of encoders				
w/ clinicalBERT [15]	89.63	92.11	59.59	59.81
w/ ResNet3D 50	90.62	92.77	62.00	62.86
On hierarchical knowledge-enhancement				
w/o all imaging-report alignments	89.27	92.27	61.46	61.50
w/o modality-wise alignment	89.87	92.07	61.40	60.68
w/o disease description query	84.62	83.64	51.73	48.29
w/o CVP	89.85	92.27	60.61	60.66
UniBrain	90.71	92.62	62.27	63.27

disease description provides more comprehensive information, allowing the text feature to pay more robust attention on the image features.

6 Discussion

6.1 Clinical Impact Analysis

UniBrain is primarily dedicated to more general brain disease diagnosis, and our experiments demonstrate that UniBrain outperforms the current state-of-the-art methods in diagnosis accuracy and interpretation. We consider UniBrain as a promising avenue for computer-aided diagnosis in brain MRI, potentially enhancing the productivity and alleviating the workload of radiologists. Additionally, the adaptable input query length of CVP enables UniBrain to seamlessly extend to a range of downstream tasks. Experiments in Section 4.6 shows the competitive performance even in challenging scenarios involving open-class and domain shift settings, thus broadening the scope of UniBrain in clinical applications.

6.2 Limitations and Future Work

Despite the effectiveness, there remains a few limitations to UniBrain: 1) the report primarily comprises abnormal observations, while the image contains both the normal and abnormal patches.

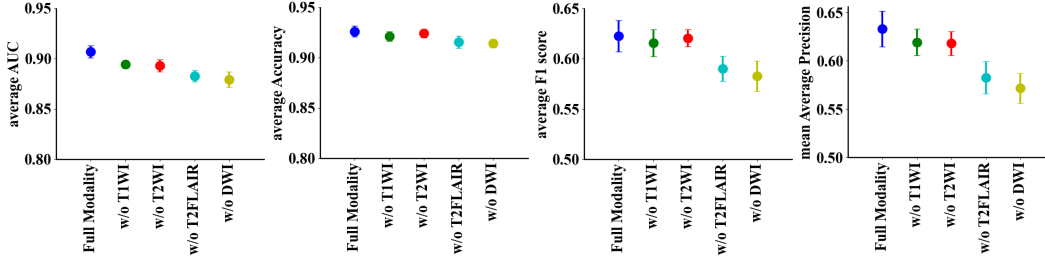


Figure 6: Comparison of full-modality with modality absence situations in terms of aAUC, aACC, aF1 and mAP.

Consequently, the current alignment of imaging and report may lead to the overfitting between normal image patches with the abnormal observations in the report. More explorations can take this point into consideration in the future to improve the alignment mechanism; 2) UniBrain can be greatly affected by the modality absence as shown in Fig. 6, which is a common problem in the real-world scenarios. As it is hard to guarantee the full modalities in some cases, it will be important to consider the robustness of the pre-training models to handle this problem. 3) UniBrain lacks the capability of the pixel-level lesion segmentation. As a prospective direction, the objective is to develop an integrated brain MRI diagnosis system that entails both classification and pixel-level lesion segmentation capabilities for multiple types of diseases.

7 Conclusion

In this work, we propose a hierarchical knowledge-enhanced pre-training framework named UniBrain for the general diagnosis of brain disorders. First, we design an automatic report decomposition method to efficiently extract the important pieces of report for pre-training. Second, we perform a hierarchical imaging-report alignment to achieve a fine-grained knowledge enhancement. Lastly, we input the global image features and disease query set into the coupled vision-language perception module to generate the final diagnosis and grounding. Experiments show UniBrain not only outperforms SOTA methods on both in-house and public datasets under open-class and domain shift settings but also yields comparable performance on certain categories compared to human experts.

References

- [1] Nagwa M. Aboelenen, Piao Songhao, Anis Koubaa, Alam Noor, and Ahmed Affi. Httu-net: Hybrid two track u-net for automatic brain tumor segmentation. *IEEE Access*, 8:101406–101415, 2020. doi: 10.1109/ACCESS.2020.2998601.
- [2] Benedikt Boecking, Naoto Usuyama, Shruthi Bannur, Daniel C Castro, Anton Schwaighofer, Stephanie Hyland, Maria Wetscherek, Tristan Naumann, Aditya Nori, Javier Alvarez-Valle, et al. Making the most of text semantics to improve biomedical vision-language processing. In *European conference on computer vision*, pages 1–21. Springer, 2022.
- [3] Tom Brown et al. Language models are few-shot learners. *Advances in neural information processing systems*, 33:1877–1901, 2020.
- [4] DH Chaihra and S Vijaya Shetty. Alzheimer’s disease detection from brain mri data using deep learning techniques. In *2021 2nd Global Conference for Advancement in Technology (GCAT)*, pages 1–5, 2021. doi: 10.1109/GCAT52182.2021.9587756.
- [5] Soumick Chatterjee, Faraz Ahmed Nizamani, Andreas Nürnbergger, and Oliver Speck. Classification of brain tumours in mr images using deep spatiotemporal models. *Scientific Reports*, 12(1): 1505, 2022.
- [6] Geeticka Chauhan, Ruizhi Liao, William Wells, Jacob Andreas, Xin Wang, Seth Berkowitz, Steven Horng, Peter Szolovits, and Polina Golland. Joint modeling of chest radiographs and radiology reports for pulmonary edema assessment. In *Medical Image Computing and Computer*

Assisted Intervention–MICCAI 2020: 23rd International Conference, Lima, Peru, October 4–8, 2020, Proceedings, Part II 23, pages 529–539. Springer, 2020.

- [7] Jieneng Chen, Yongyi Lu, Qihang Yu, Xiangde Luo, Ehsan Adeli, Yan Wang, Le Lu, Alan L Yuille, and Yuyin Zhou. Transunet: Transformers make strong encoders for medical image segmentation. *arXiv preprint arXiv:2102.04306*, 2021.
- [8] Sihong Chen, Jing Qin, Xing Ji, Baiying Lei, Tianfu Wang, Dong Ni, and Jie-Zhi Cheng. Automatic scoring of multiple semantic attributes with multi-task feature leverage: a study on pulmonary nodules in ct images. *IEEE transactions on medical imaging*, 36(3):802–814, 2016.
- [9] Sihong Chen, Kai Ma, and Yefeng Zheng. Med3d: Transfer learning for 3d medical image analysis. *arXiv preprint arXiv:1904.00625*, 2019.
- [10] Alessandro Crimi and Spyridon Bakas, editors. *Brainlesion: Glioma, Multiple Sclerosis, Stroke and Traumatic Brain Injuries - 5th International Workshop, BrainLes 2019, Held in Conjunction with MICCAI 2019, Shenzhen, China, October 17, 2019, Revised Selected Papers, Part II*, volume 11993 of *Lecture Notes in Computer Science*, 2020. Springer.
- [11] Yin Dai et al. Transmed: Transformers advance multi-modal medical image classification. *Diagnostics*, 11(8):1384, 2021.
- [12] Leyuan Fang, Chong Wang, Shutao Li, Hossein Rabbani, Xiangdong Chen, and Zhimin Liu. Attention to lesion: Lesion-aware convolutional neural network for retinal optical coherence tomography image classification. *IEEE transactions on medical imaging*, 38(8):1959–1970, 2019.
- [13] Yu Gu, Robert Tinn, Hao Cheng, Michael Lucas, Naoto Usuyama, Xiaodong Liu, Tristan Naumann, Jianfeng Gao, and Hoifung Poon. Domain-specific language model pretraining for biomedical natural language processing. *ACM Transactions on Computing for Healthcare (HEALTH)*, 3(1):1–23, 2021.
- [14] Ali Hatamizadeh, Yucheng Tang, Vishwesh Nath, Dong Yang, Andriy Myronenko, Bennett Landman, Holger R Roth, and Daguang Xu. Unetr: Transformers for 3d medical image segmentation. In *Proceedings of the IEEE/CVF winter conference on applications of computer vision*, pages 574–584, 2022.
- [15] Kexin Huang et al. Clinicalbert: Modeling clinical notes and predicting hospital readmission. *arXiv preprint arXiv:1904.05342*, 2019.
- [16] Shih-Cheng Huang, Liyue Shen, Matthew P Lungren, and Serena Yeung. Gloria: A multimodal global-local representation learning framework for label-efficient medical image recognition. In *Proceedings of the IEEE/CVF International Conference on Computer Vision*, pages 3942–3951, 2021.
- [17] Xin Huang et al. Dual-ray net: automatic diagnosis of thoracic diseases using frontal and lateral chest x-rays. *Journal of Medical Imaging and Health Informatics*, 10(2):348–355, 2020.
- [18] Sarfaraz Hussein, Kunlin Cao, Qi Song, and Ulas Bagci. Risk stratification of lung nodules using 3d cnn-based multi-task learning. In *Information Processing in Medical Imaging: 25th International Conference, IPMI 2017, Boone, NC, USA, June 25-30, 2017, Proceedings 25*, pages 249–260. Springer, 2017.
- [19] Jeremy Irvin, Pranav Rajpurkar, Michael Ko, Yifan Yu, Silvana Ciurea-Ilcus, Chris Chute, Henrik Marklund, Behzad Haghgoo, Robyn Ball, Katie Shpanskaya, et al. Chexpert: A large chest radiograph dataset with uncertainty labels and expert comparison. In *Proceedings of the AAAI conference on artificial intelligence*, volume 33, pages 590–597, 2019.
- [20] Eunji Jun, Seungwoo Jeong, Da-Woon Heo, and Heung-II Suk. Medical transformer: Universal brain encoder for 3d mri analysis. *arXiv preprint arXiv:2104.13633*, 2021.
- [21] Girish Katti, Syeda Arshiya Ara, and Ayesha Shireen. Magnetic resonance imaging (mri)–a review. *International journal of dental clinics*, 3(1):65–70, 2011.

- [22] Jason P Lerch, André JW Van Der Kouwe, Armin Raznahan, Tomáš Paus, Heidi Johansen-Berg, Karla L Miller, Stephen M Smith, Bruce Fischl, and Stamatios N Sotiropoulos. Studying neuroanatomy using mri. *Nature neuroscience*, 20(3):314–326, 2017.
- [23] Jiangyun Li, Wenxuan Wang, Chen Chen, Tianxiang Zhang, Sen Zha, Jing Wang, and Hong Yu. Transbtsv2: Towards better and more efficient volumetric segmentation of medical images. *arXiv preprint arXiv:2201.12785*, 2022.
- [24] Liu Li et al. Attention based glaucoma detection: A large-scale database and cnn model. In *Proceedings of the IEEE/CVF conference on computer vision and pattern recognition*, pages 10571–10580, 2019.
- [25] Chin-Fu Liu, Johnny Hsu, Xin Xu, Sandhya Ramachandran, Victor Wang, Michael I Miller, Argye E Hillis, and Andreia V Faria. Deep learning-based detection and segmentation of diffusion abnormalities in acute ischemic stroke. *Communications Medicine*, 1(1):61, 2021.
- [26] Lihao Liu, Zhening Huang, Pietro Liò, Carola-Bibiane Schönlieb, and Angelica I Aviles-Rivero. Pc-swinmorph: Patch representation for unsupervised medical image registration and segmentation. *arXiv preprint arXiv:2203.05684*, 2022.
- [27] Matthew BA McDermott, Tzu Ming Harry Hsu, Wei-Hung Weng, Marzyeh Ghassemi, and Peter Szolovits. Chexpert++: Approximating the chexpert labeler for speed, differentiability, and probabilistic output. In *Machine Learning for Healthcare Conference*, pages 913–927. PMLR, 2020.
- [28] Masahiro Mitsuhashi et al. Embedding human knowledge into deep neural network via attention map. *arXiv preprint arXiv:1905.03540*, 2019.
- [29] Yifan Peng, Xiaosong Wang, Le Lu, Mohammadhadi Bagheri, Ronald Summers, and Zhiyong Lu. Negbio: a high-performance tool for negation and uncertainty detection in radiology reports. *AMIA Summits on Translational Science Proceedings*, 2018:188, 2018.
- [30] Alec Radford, Jong Wook Kim, Chris Hallacy, Aditya Ramesh, Gabriel Goh, Sandhini Agarwal, Girish Sastry, Amanda Askell, Pamela Mishkin, Jack Clark, et al. Learning transferable visual models from natural language supervision. In *International conference on machine learning*, pages 8748–8763. PMLR, 2021.
- [31] Val M Runge, Shigeki Aoki, William G Bradley Jr, Kee-Hyun Chang, Marco Essig, Lin Ma, Jeffrey S Ross, and Anton Valavanis. Magnetic resonance imaging and computed tomography of the brain—50 years of innovation, with a focus on the future. *Investigative radiology*, 50(9): 551–556, 2015.
- [32] Akshay Smit et al. Chexpert: combining automatic labelers and expert annotations for accurate radiology report labeling using bert. *arXiv preprint arXiv:2004.09167*, 2020.
- [33] Jiaying Tan, Yumei Huo, Zhengrong Liang, and Lihong Li. Expert knowledge-infused deep learning for automatic lung nodule detection. *Journal of X-ray Science and Technology*, 27(1): 17–35, 2019.
- [34] Yucheng Tang, Dong Yang, Wenqi Li, Holger R Roth, Bennett Landman, Daguang Xu, Vishwesh Nath, and Ali Hatamizadeh. Self-supervised pre-training of swin transformers for 3d medical image analysis. In *Proceedings of the IEEE/CVF Conference on Computer Vision and Pattern Recognition*, pages 20730–20740, 2022.
- [35] Ekin Tiu, Ellie Talius, Pujan Patel, Curtis P Langlotz, Andrew Y Ng, and Pranav Rajpurkar. Expert-level detection of pathologies from unannotated chest x-ray images via self-supervised learning. *Nature Biomedical Engineering*, 6(12):1399–1406, 2022.
- [36] Du Tran et al. Learning spatiotemporal features with 3d convolutional networks. In *Proceedings of the IEEE international conference on computer vision*, pages 4489–4497, 2015.
- [37] Ashish Vaswani, Noam Shazeer, Niki Parmar, Jakob Uszkoreit, Llion Jones, Aidan N Gomez, Łukasz Kaiser, and Illia Polosukhin. Attention is all you need. *Advances in neural information processing systems*, 30, 2017.

- [38] Kun Wang et al. Learning to recognize thoracic disease in chest x-rays with knowledge-guided deep zoom neural networks. *IEEE Access*, 8:159790–159805, 2020.
- [39] Chaoyi Wu, Xiaoman Zhang, Yanfeng Wang, Ya Zhang, and Weidi Xie. K-diag: Knowledge-enhanced disease diagnosis in radiographic imaging. *arXiv preprint arXiv:2302.11557*, 2023.
- [40] Chaoyi Wu, Xiaoman Zhang, Ya Zhang, Yanfeng Wang, and Weidi Xie. Medklip: Medical knowledge enhanced language-image pre-training. *medRxiv*, pages 2023–01, 2023.
- [41] Yixuan Wu et al. D-former: A u-shaped dilated transformer for 3d medical image segmentation. *Neural Computing and Applications*, 35(2):1931–1944, 2023.
- [42] Madeleine K Wyburd et al. Teds-net: enforcing diffeomorphisms in spatial transformers to guarantee topology preservation in segmentations. In *International Conference on Medical Image Computing and Computer-Assisted Intervention*, pages 250–260. Springer, 2021.
- [43] Xiaozheng Xie, Jianwei Niu, Xuefeng Liu, Zhengsu Chen, Shaojie Tang, and Shui Yu. A survey on incorporating domain knowledge into deep learning for medical image analysis. *Medical Image Analysis*, 69:101985, 2021.
- [44] Yutong Xie, Yong Xia, Jianpeng Zhang, Yang Song, Dagan Feng, Michael Fulham, and Weidong Cai. Knowledge-based collaborative deep learning for benign-malignant lung nodule classification on chest ct. *IEEE transactions on medical imaging*, 38(4):991–1004, 2018.
- [45] Shujun Zhang, Shuhao Xu, Liwei Tan, Hongyan Wang, and Jianli Meng. Stroke lesion detection and analysis in mri images based on deep learning. *Journal of Healthcare Engineering*, 2021: 1–9, 2021.
- [46] Xiaoman Zhang, Chaoyi Wu, Ya Zhang, Yanfeng Wang, and Weidi Xie. Knowledge-enhanced pre-training for auto-diagnosis of chest radiology images. *arXiv preprint arXiv:2302.14042*, 2023.
- [47] Yao Zhang et al. mmformer: Multimodal medical transformer for incomplete multimodal learning of brain tumor segmentation. In *Medical Image Computing and Computer Assisted Intervention – MICCAI 2022*, pages 107–117, Cham, 2022. Springer Nature Switzerland.
- [48] Yuhao Zhang, Hang Jiang, Yasuhide Miura, Christopher D Manning, and Curtis P Langlotz. Contrastive learning of medical visual representations from paired images and text. In *Machine Learning for Healthcare Conference*, pages 2–25. PMLR, 2022.
- [49] Bolei Zhou, Aditya Khosla, Agata Lapedriza, Aude Oliva, and Antonio Torralba. Learning deep features for discriminative localization. In *Proceedings of the IEEE conference on computer vision and pattern recognition*, pages 2921–2929, 2016.
- [50] Lei Zhou, Huidong Liu, Joseph Bae, Junjun He, Dimitris Samaras, and Prateek Prasanna. Self pre-training with masked autoencoders for medical image classification and segmentation. *arXiv preprint arXiv:2203.05573*, 2022.